A New Approach to Probe the Degradation of Fuel Cell Catalysts under Realistic Conditions: Combining Tests in a Gas Diffusion Electrode Setup with Small Angle X-ray Scattering

Journal of The Electrochemical Society, 2020 **167** 134515
1945-7111/2020/167(13)/134515/8/$40.00 © 2020 The Electrochemical Society ("ECS"). Published on behalf of ECS by IOP Publishing Limited

A New Approach to Probe the Degradation of Fuel Cell Catalysts under Realistic Conditions: Combining Tests in a Gas Diffusion Electrode Setup with Small Angle X-ray Scattering

Johanna Schröder,[1,2] Jonathan Quinson,[3] Jette K. Mathiesen,[3] Jacob J. K. Kirkensgaard,[4] Shima Alinejad,[1] Vladislav A. Mints,[1] Kirsten M. ∅. Jensen,[3] and Matthias Arenz[1,*,z]

[1]*Department of Chemistry and Biochemistry, University of Bern, 3012 Bern, Switzerland*
[2]*Institute of Applied and Physical Chemistry (IAPC), Center for Environmental Research and Sustainable Technology, University of Bremen, 28359 Bremen, Germany*
[3]*Department of Chemistry, University of Copenhagen, 2100 Copenhagen, Denmark*
[4]*Department of Food Science, University of Copenhagen, 958 Frederiksberg, Denmark*

A new approach for efficiently investigating the degradation of fuel cell catalysts under realistic conditions is presented combining accelerated stress tests (ASTs) in a gas diffusion electrode (GDE) setup with small angle X-ray scattering (SAXS). GDE setups were recently introduced as a novel testing tool combining the advantages of classical electrochemical cells with a three-electrode setup and membrane electrode assemblies (MEAs). SAXS characterization of the catalyst layer enables an evaluation of the particle size distribution of the catalyst and its changes upon applying an AST. The straight-forward approach not only enables stability testing of fuel cell catalysts in a comparative and reproducible manner, it also allows mechanistic insights into the degradation mechanism. Typical metal loadings for proton exchange membrane fuel cells (PEMFCs), i.e. 0.2 mg_{Pt} cm^{-2}_{geo}, are applied in the GDE and the degradation of the overall (whole) catalyst layer is probed. For the first time, realistic degradation tests can be performed comparing a set of catalysts with several repeats within reasonable time. It is demonstrated that independent of the initial particle size in the pristine catalyst, for ASTs simulating load cycle conditions in a PEMFC, all catalysts degrade to a similar particle size distribution.
 [DOI: 10.1149/1945-7111/abbdd2]

Manuscript submitted May 12, 2020; revised manuscript received September 10, 2020. Published October 12, 2020.

Supplementary material for this article is available online

Proton exchange membrane fuel cells (PEMFCs) are a promising alternative to replace combustion engines[1–3] with the development of fuel-cells vehicles. A key component of this technology are using nanoparticles (NPs), nowadays typically Pt-alloys (e.g. PtCo in the Mirai automobile from Toyota),[4–6] supported on high surface carbon as catalysts.[3] For a long time, the main research focus was to improve the catalyst activity leading to the development of several different types of highly active catalysts.[7] More recently, the performance at high current densities and the effect of high oxygen mass transfer resistances has gained increasing attention.[8] It was established that the oxygen mass transfer resistance decreases by increasing the metal dispersion on the support material, i.e. the decrease in particle size of the catalyst.[8] However, besides a high activity, a sufficient stability of the catalysts is required for applications.[1,9] Today, most degradation studies are either performed under idealized conditions, or they lack statistics and comparative character. Hence an efficient, i.e. fast and realistic, testing of fuel cell catalysts is needed to bridge catalyst development to their application in fuel cells. Ideally the testing is not of pure descriptive behavior, but also mechanistic insights are provided.

To simulate the use of catalysts under realistic conditions and at the same time accelerate their degradation, stability investigations are performed using accelerated stress tests (AST), e.g. following protocols recommended by the Fuel Cell Commercialization Conference of Japan (FCCJ).[10,11] Usually such measurements are either performed in classical electrochemical cells with a three-electrode setup[12] or in membrane electrode assemblies (MEAs).[13] Both approaches have advantages and disadvantages. Classic electrochemical cells enable relatively fast screening at the expense of a somewhat unrealistic "environment" (e.g. liquid electrolyte). MEAs offer a more realistic "environment" but require significantly more advanced facilities such as a complete hydrogen infrastructure in the laboratory. In addition, MEA testing is very time consuming and therefore usually not combined with spectroscopic tools in a comparative manner, i.e. comparing different catalysts and showing several repeats for each sample. A powerful methodology to combine the advantages of both approaches for an efficient testing fuel cell catalysts under realistic conditions is the gas diffusion electrode (GDE) setup.[14,15] Alinejad et al.[15] recently presented the benefits to perform AST protocols in gas diffusion setups by following the loss in catalyst active surface area as function of the electrochemical treatment.

In the here presented work, a significant advancement of this approach is achieved by using realistic catalyst layers applied in MEA testing and by combining such tests with the analysis of the catalyst layer via small angle X-ray scattering (SAXS). The known electrochemical degradation mechanisms of (1) migration of particles followed by coalescence and potentially sintering, (2) metal dissolution, (3) electrochemical Ostwald ripening, where large particles grow at the expense of small ones, and (4) particle detachment from the support[16] have a direct effect on the particle size distribution of the catalysts. The understanding of the degradation mechanism is key to propose and develop mitigation strategies. Commonly, the determination of the particle size is done by (scanning) transmission electron microscopy ((S)TEM) and to observe the change of selected particles before and after the treatment identical location (IL) (S)TEM is performed using rotating disk electrode (RDE)[16–18] or GDE setups.[15] However, while (S)TEM is a local method, SAXS offers the benefits to analyze the particle size distribution after performing the AST in the whole catalyst layer[19,20] and even without further dismantling of the GDE as we demonstrate in the present study. In the present work, load-cycle conditions were simulated in an AST protocol by applying potential steps between 0.6 and 1.0 V_{RHE} in oxygen saturated atmosphere at 25 °C and 50 °C in a GDE setup. The combination of electrochemical measurements and SAXS analysis allows to determine the loss in active surface area and to relate it to a change in particle size as function of operation temperature and initial NP size distribution. We demonstrate with this study that the combination of GDE and SAXS is an efficient way to test fuel cell catalysts in a comparative manner under realistic conditions and enable mechanistic insights into the catalyst degradation.

*Electrochemical Society Member.
[z]E-mail: matthias.arenz@dcb.unibe.ch

Experimental

Chemicals, materials, and gases.—Ultrapure Milli-Q water (resistivity > 18.2 MΩ·cm, total organic carbon (TOC) < 5 ppb) from a Millipore system was used for catalyst ink formation, diluting the acid, and the cleaning of the GDE cell. For preparing the catalysts ink isopropanol (IPA, 99.7 + %, Alfa Aesar), commercial Pt/C catalysts (TEC10E20A (1–2 nm Pt/C, 19.4 wt% Pt), TEC10E50E (2–3 nm Pt/C, 46.0 wt% Pt), TEC10E50E-HT (4–5 nm Pt/C, 50.6 wt% Pt), Tanaka kikinzoku kogyo), and Nafion dispersion (D1021, 10 wt.%, EW 1100, Fuel Cell Store) was used.

The GDE was prepared using a Nafion membrane (Nafion 117, 183 μm thick, Fuel Cell Store), two gas diffusion layers (GDL) (Sigracet 39AA, 280 μm thick, Fuel Cell Store; with a microporous layer (MPL): Sigracet 39BC, 325 μm thick, Fuel Cell Store). In this study the Nafion membrane was always pretreated. Circles with a diameter of 2 cm were cut from a sheet of Nafion membrane. Those cutoff membranes were treated in 5 wt.% H_2O_2 (Hänseler, 30 min, 80 °C), rinsed with Milli-Q water, treated in Milli-Q water (30 min, 80 °C), rinsed again with Milli-Q water, and treated in 8 wt.% H_2SO_4 (30 min, 80 °C). After final rinsing of the cutoff membranes with Milli-Q water, they were kept in a glass vial filled with Milli-Q water.

Diluted 70% perchloric acid ($HClO_4$, 99.999% trace metals basis, Sigma Aldrich) as electrolyte and the gases Ar (99.999%), O_2 (99.999%), and CO (99.97%) from Air Liquide were used in the electrochemical measurements.

Gas diffusion electrode setup.—An in-house gas diffusion electrode setup as described before[14,15] was used in the electrochemical measurements. The GDE was placed on top of the flow field in the stainless-steel cell body with the Nafion membrane upwards. The upper cell part above the Nafion membrane is made of polytetrafluoroethylene (PTFE). A platinum wire was used as a counter electrode (CE) and a reversible hydrogen electrode (RHE) as a reference electrode (RE). The CE was placed inside a glass capillary with a glass frit on the bottom to avoid the trapping of gas bubbles in the hole of the Teflon cell and hence helping to improve the reproducibility of the measurement. All potentials in this study are referred to the RHE potential.

In an initial cleaning the Teflon upperpart was soaked in acid (H_2SO_4:HNO_3 = 1:1, v:v) overnight. After rinsing it with ultrapure water, it was boiled twice in ultrapure water. Between the measurements the Teflon upper part, the RE, and the glass capillary were boiled once in ultrapure water.

Catalyst synthesis and ink formation.—Three commercial Tanaka catalysts with different particle sizes and metal loadings were used. The ink was formed by dispersing the catalysts in a mixture of Milli-Q water and IPA (water/IPA ratio of 3:1) to obtain about 5 ml of ink with a Pt concentration of 0.5 mg ml^{-1}. The mixture was sonicated for 5 min in a sonication bath to get a suitable dispersion. 23–98 μl of Nafion was added (Nafion/carbon mass ratio of 1). The dispersion was again sonicated for 5 min in a sonication bath.

Vacuum filtration and pressing of GDE.—The Sigracet 39BC gas diffusion layer (GDL) was placed in a vacuum filtration setup between a glass funnel and a sand core filter. All this was placed on a collecting bottle as described by Yarlagadda et al.[21] 4 ml of the inks were diluted with 7 ml of Milli-Q water and 29 ml of IPA (water-IPA ratio of 1:3, Pt concentration of 0.05 mg l^{-1}). The mixture was sonicated for 1 min. The 40 ml diluted ink were filled in a funnel. A jet water pump was used to deposit the catalyst on top of the GDL. When the collected solvent was not colorless it was refilled into the funnel and the vacuum filtration was started again. Afterwards, the GDE was dried at least overnight on air. By this procedure a theoretical Pt loading of 0.208 mg_{Pt} $cm^{-2}{}_{geo}$ was generated.

The Nafion membrane was pressed on top of the GDE. Therefore, a Teflon sheet was placed on top of a Teflon block and afterwards the GDL without MPL (∅ 2 cm), GDL with MPL (∅ 2 cm with hole of ∅ 3 mm) and the catalyst on the GDL from the vacuum filtration (∅ 3 mm) in the hole. A Nafion membrane (to avoid later the leaking of the electrolyte into the GDE) was rinsed with Milli-Q water, dried and followed by a second Teflon sheet and a second Teflon block placed on top. Everything was placed between two metal blocks and the pressing was performed at 2 tons for 10 min.

Electrochemical measurement.—The electrochemical measurements were performed with a computer controlled parallel potentiostat (ECi-242, NordicElectrochemistry). Two measurements could be performed in parallel by splitting the gas inlet after humidification of the gas. Hence the gas inlet of two GDE setups was connected to the same bubbler. 4 M $HClO_4$ aqueous solution in the upper Teflon compartment of the GDE setup was used as electrolyte and different temperatures (25 °C or 50 °C) were applied using a fan in an isolated Faraday cage. Before performing the AST protocols first 20 cyclic voltammograms (CVs) in Argon (Ar, with a scan rate of 500 mV s^{-1}, 0.06–1.1 V_{RHE}) were performed to assess if the assembling of the cell was successful. For cleaning the surface, afterwards CVs in oxygen (O_2) were performed: 20 CVs with 500 mV s^{-1}, then ca. 50 CVs with 50 mV s^{-1} until a stable CV was obtained. The resistance between the working electrode (WE) and RE (ca. 10 Ω) was compensated to around 2 Ω by using the analog positive feedback scheme of the potentiostat. The resistance was determined online using an AC signal (5 kHz, 5 mV)[22] Before starting the measurement, to make sure that the O_2 was completely replaced, CVs in Ar (50 CVs, 500 mV s^{-1}) were done. The wished temperature for the following AST was adjusted.

To investigate the degradation mechanism(s) of the Pt/C electrocatalysts, ASTs as reported by Alinejad et al.[15] were used. The applied electrode potential was stepped between 0.6 and 1.0 V_{RHE} and hold for three seconds, respectively to simulate the load-cycle conditions. The surface loss of the catalysts during the AST was determined by comparing the ECSA obtained from the CO stripping voltammetry before and after the AST of at least three reproducible measurements. The ECSA values in m^2 $g_{Pt}{}^{-1}$ were determined using the theoretical Pt loading of 0.208 mg_{Pt} $cm^{-2}{}_{geo}$ and the surface area (in cm^2) determined by CO stripping. The CO stripping was performed by subtracting the Ar background and using a baseline correction between the chosen peak limits to avoid any influence of capacitive currents from the carbon support as shown by Inaba et al.[23] ASTs were performed in O_2 with 9000 steps at 25 °C or 5000 steps at 50 °C.

SAXS analysis.—A SAXSLab instrument (Niels Bohr Institute, University of Copenhagen, Denmark) equipped with a 100XL + micro-focus sealed X-ray tube (Rigaku) producing a photon beam with a wavelength of 1.54 Å was used for SAXS data acquisition.[20,24] A 2D 300 K Pilatus detector from Dectris was used to record the scattering patterns and the samples did not show anisotropy. The two-dimensional scattering data were azimuthally averaged, normalized by the incident radiation intensity, the sample exposure time and the transmission using the Saxsgui software. Data were then corrected for background and detector inhomogeneities using standard reduction software. Samples were sealed between two 5–7 μm thick mica windows in dedicated sample cells and measurements performed in vacuum. The background measurement was made with a GDL Sigracet 39BC without NPs.

The radially averaged intensity I(q) is given as a function of the scattering vector $q = 4\pi\cdot\sin(\theta)/\lambda$, where λ is the wavelength and 2θ is the scattering angle. The background corrected scattering data were fitted using a power law to take into account the behavior at low q value and a model of polydisperse spheres described by a volume-weighted log-normal distribution. This model leads to satisfying results for 13 samples out of 36 samples. The remaining data were then best fitted by adding a second model of polydisperse

spheres also described by a volume-weighted log-normal distribution (for 11 samples out of 36). A structure factor contribution was sometimes needed to properly model the data for the 2 polydisperse sphere models (6 samples out of 36). We employed a hard-sphere structure factor $F(R,\eta)$ as described in Ref. 25. The scattering data are fitted to the following general expression:

$$I(q) = A \cdot q^{-n} + C_1 \cdot F(R_1, \eta_1) \cdot \int P_{S1}(q, R) V_1(R) D_1(R) dR + C_2 \int P_{S2}(q, R) V_2(R) D_2(R) dR$$

where $A \cdot q^{-n}$ corresponds to the power law where A and n are free parameters; C_1 and C_2 are scaling constants, Ps_1 and Ps_2 the sphere form factors, V_1 and V_2 the particle volumes and D_1 and D_2 the log-normal size distribution. The sphere form factor is given by[26,27]:

$$Ps(q, R) = \left(3\frac{\sin(qR) - qR\cos(qR)}{(qR)^3}\right)^2$$

and the log-normal distribution by:

$$D(R) = \frac{1}{R\sigma\sqrt{2\pi}} \exp\left(\frac{-\left[\ln\left(\frac{R}{R_0}\right)\right]^2}{2\sigma^2}\right)$$

where σ is the variance and R_0 the geometric mean of the log-normal distribution. The fitting was done using home written MATLAB code. The free parameters in the model are: A, n, R_1, R_2, σ_1, σ_2, C_1, C_2, η_1. The values obtained for these parameters are reported in Table SI. In 13 out 36 samples, only 5 free parameters where needed, and a one population model was enough to describe the sample. For 3 samples a model adding a structure factor with 6 free parameters gave a better fit. After ASTs however and in particular for the initially 1–2 nm Pt/C catalysts, better fits were obtained with 8 free parameters considering 2 spheres populations. In 3 cases a better fit was obtained with 9 free parameters. In order to account for the two populations, the reported probability density functions were weighted by the relative surface contribution of the spheres as detailed in SI. The scattering data and corresponding fits are reported in Figs. S1–S4 (available online at stacks.iop.org/JES/167/134515/mmedia) and Table SI. In the discussion, we refer to the average diameter of the particle and use the standard deviation relative to the evaluation of this average diameter based on three independent measurements as error to compare the catalyst sizes. In other words, the values quoted in the manuscript read as $\langle d \rangle \pm \sigma_{\langle d \rangle}$ where $\langle d \rangle$ is the average diameter retrieved from three independent measurements and $\sigma_{\langle d \rangle}$ a measure of how reproducible this estimation of $\langle d \rangle$ is from three independent measurements. The relative deviation relative to $\langle d \rangle$ (σ_d), i.e. how broad the distribution is around the value $\langle d \rangle$, was between 10 and 30%, see details in Table SI.

The "starting size" was analyzed from three samples of 3 mm diameter punched from catalyst film on the GDL after vacuum filtration. Three samples with reproducible ECSAs after the AST were analyzed by punching a circle with a diameter of 5 mm around the GDE (of 3 mm) with the Nafion membrane on top. The background sample was obtained by performing the AST protocol on a catalyst free "GDE" by using a circle with a diameter of 3 mm Sigracet 39BC as "GDE" (pressing was performed the same way as before).

TEM analysis.—TEM micrographs were obtained using a Jeol 2100 operated at 200 kV. Samples were characterized by imaging at least 5 different areas of the TEM grid at minimum 3 different magnifications. The size (diameter) of the NPs was estimated using the imageJ software and considering at least 200 NPs. The samples Pt/C were diluted in ethanol before being drop casted onto a holey carbon support film of Cu 300 mesh grids (Quantifoil).

Pair distribution function (PDF) analysis.—Data acquisition: X-ray total scattering data were obtained at beamline 11-ID-B, Advanced Photon Source (APS), Argonne National Laboratory, USA. The samples were mounted on a flat plate sample holder, so that data were collected in transmission geometry using a Perkin-Elmer flat panel detector with a pixel size of 200 × 200 μm in the RA-PDF setup.[28] A wavelength of 0.2115 Å was used, and the sample-to-detector distance was calibrated using a CeO_2 standard. Fit2D was used to calibrate the experimental geometry parameters and azimuthally integrate the scattering intensities to 1D scattering patterns.[29,30]

PDF modelling: X-ray total scattering data were Fourier transformed with xPDFsuite to obtain PDFs using the Q-range from 0.9 Å −1 to 22.0 Å−1.[31] The scattering signal from the carbon substrate and Nafion membrane was subtracted before the Fourier transform. The scattering signal from the carbon substrate was measured independently, while that from the MEA membrane was determined from the data obtained from the largest nanoparticles after O_2 exposure by subtracting out the well-known Pt contribution in reciprocal space. Analysis and refinement of the obtained PDFs was performed using PDFgui, in which a least-square optimization procedure is performed between a theoretical PDF and the experimental PDF from a model.[32] The refined parameters included the unit cell, d2-parameter describing local correlated atomic movement, scale factor, a spherical particle diameter and the atomic displacement parameters (ADPs) for Pt.

Results and Discussion

An efficient catalyst testing must be fast, performed under realistic conditions, and conducted to allow several repeats for each catalyst sample. To assess the Pt NP size evolution in Pt/C catalysts, SAXS is so far mainly used in combination with RDE testing in addition to the local technique (S)TEM.[19,20] Although single RDE measurements are fast, the testing conditions are far from the ones in fuel cell devices[14,15]; a liquid electrolyte is employed, which respective type of anions[33–35] and pH values[36,37] influence Pt dissolution while the catalyst film thickness (loading on the glassy carbon tip) is significantly lower than in a fuel cell. Furthermore, to reach sufficient signal to noise ratios for the SAXS analysis, the catalyst layer must be collected from several RDE measurements. This renders the study of the effect of stability tests on the NP size impractical and time consuming. The conditions in MEA testing are realistic but time consuming and rarely performed with several repeats of different catalysts. Among the very few in situ SAXS studies reported, most require exposure of the electrocatalyst to liquid electrolyte flow or are performed in a MEA.[38–44] In setups exposing the catalyst to liquid electrolyte flow the risk of a mechanical delamination and incomplete catalyst utilization is given. For an analysis of the catalyst layers in MEA, a dismantling is necessary to avoid probing anode and cathode catalyst at the same time. Due to the complexity of the experiments and the limited measurement time at Synchrotron beamlines, to the best of our knowledge in no in situ SAXS study statistical data concerning the reproducibility of the measurements is tested by performing three repeats per sample. These limitations call for further improvement.

In contrast, the GDE setup provides more realistic conditions than the RDE method but is at the same time a more simple and faster methodology than flow cell or MEA measurements.[14,15] Several repeats of the measurements can be performed and their reproducibility be discussed. Therefore, in this work, a GDE setup is used to investigate the degradation of three commercial Tanaka Pt/C catalysts with different NP size distributions ranging from 1–2 to 4–5 nm (hereafter denoted as 1–2 nm Pt/C, 2–3 nm Pt/C, and 4–5 nm Pt/C) that are often used as benchmark catalysts in RDE testing.[45]

TEM micrographs of the three catalyst powders are displayed in Fig. 1. In a recent work we showed that ASTs can be performed in our GDE setup but the used catalyst loading was comparable to loadings for RDE measurements and hence far from realistic fuel cell loadings.[15] In the present work, the catalyst film on the GDL (i.e. the GDE) is prepared by vacuum filtration as described by Yarlagadda et al.[21] to reach typical catalyst loadings for fuel cells in cars of 0.2 mg_{Pt} cm^{-2}_{geo}.[8] ASTs are performed at 25 °C (9000 steps in O_2 between 0.6 and 1.0 V_{RHE}, 3 s holding) and additionally at 50 ° C (with a reduced number of degradation steps to 5000 to reach a comparable loss in surface area) to generate more realistic fuel cell conditions.[4] In the SI it is demonstrated that with the established procedure, reproducible particle size distributions of the different Pt/C catalysts could be determined before (Fig. S5) as well as after the ASTs (Fig. S6). The same reproducibility is observed for the determined values of the electrochemically active surface area (ECSA), see relatively low standard deviations from the measurements of three catalyst films in Table I. By analyzing the electrochemical measurements recorded in the GDE setup, (Fig. 2 and Table I) and comparing the ECSA values of the catalysts with the ones reported from RDE measurements in literature it is further confirmed that the catalyst layer is fully utilized.[45] This is of utmost importance for the SAXS analysis, which otherwise would be misleading as parts of the catalyst layer that were not be under electrochemical control would not be subjected to any degradation and hence would not show any change in the particle size distributions. In addition, it is observed that going from 25 °C to 50 °C, the peak potential of the CO stripping is shifted to lower electrode potentials and the established initial ECSA is slightly reduced (see Fig. 2 and Table I). This finding is in agreement with the expected effect of higher temperature reducing the equilibrium coverage of adsorbents and facilitating the oxidation of CO.[46] Based on the average of the mean particle sizes obtained from SAXS data analyses "theoretical" surface areas before the AST can be calculated (see Table SIII in SI). Comparing the experimental ECSA established by the CO stripping and "theoretical" surface areas uncovers that although large NPs have in total less surface area, a higher fraction of the surface area is accessible for catalytic reactions as compared to the small NPs.

As prepared, the catalysts with the smaller NPs exhibit higher initial ECSA than the catalyst with larger NPs (see Table I). At the same time, the smaller NPs experience a larger ECSA loss upon applying the AST: 43 ± 1 and 34 ± 1% for 1–2 and 2–3 nm Pt/C, respectively as compared to 4 ± 1% for 4–5 nm Pt/C at 25 °C. An increase in temperature accelerates the loss in ECSA considerably (AST duration of 10 h at 50 °C as compared to 16 h 40 at 25 °C). Interestingly, the 4–5 nm Pt/C catalyst is very stable. Its ECSA loss upon applying the AST is very small, i.e. after more than 16 h of AST at 25 °C it is less than 5% and thus almost negligible. Increasing the temperature to 50 °C, the ECSA loss increases to 16% (note that the testing time was shorter, i.e. 10 h), but is still minor as compared to the ECSA loss of the 1–2 and 2–3 Pt/C catalysts of 53 ± 1 and 48 ± 2%, respectively. Another highly important observation results from a comparison of the ECSA loss at 25 °C (see Fig. 2). In our previous study by Alinejad et al.,[15] we used the same AST protocol but significantly lower catalyst loadings on the GDL. With catalyst loadings typical for RDE testing[47] (i.e. ca. 8 $\mu g\ cm^{-2}_{geo}$ vs 0.2 $mg\ cm^{-2}_{geo}$ here), significantly higher ECSA losses are observed, i.e. 48 ± 2% with lower loading as compared to 34 ± 1% in this study for the 2–3 nm Pt/C catalyst and 18 ± 1% with lower loading as compared to 4 ± 1% here for the 4–5 nm Pt/C catalyst (see Table I and Figs. S5–S6). Such dependence of the degradation on the film thickness was observed previously in our laboratory in RDE measurements (not published) as well as in Pt dissolution measurements determined via scanning flow cell (SFC) measurements coupled to inductively coupled plasma mass spectrometry (ICP-MS).[48,49] The influence of the catalyst film thickness on the observed Pt dissolutions rates was assigned to differences in the probability of re-deposition of the Pt ions.[48] The influence of different iR-drops for different catalyst loadings is considered to be small. An active compensation scheme of the potentiostat allows to limit the uncompensated resistance to similar, reproducible values (see electrochemical measurements in experimental part). However, as larger currents are obtained with a thicker catalyst layer, the same

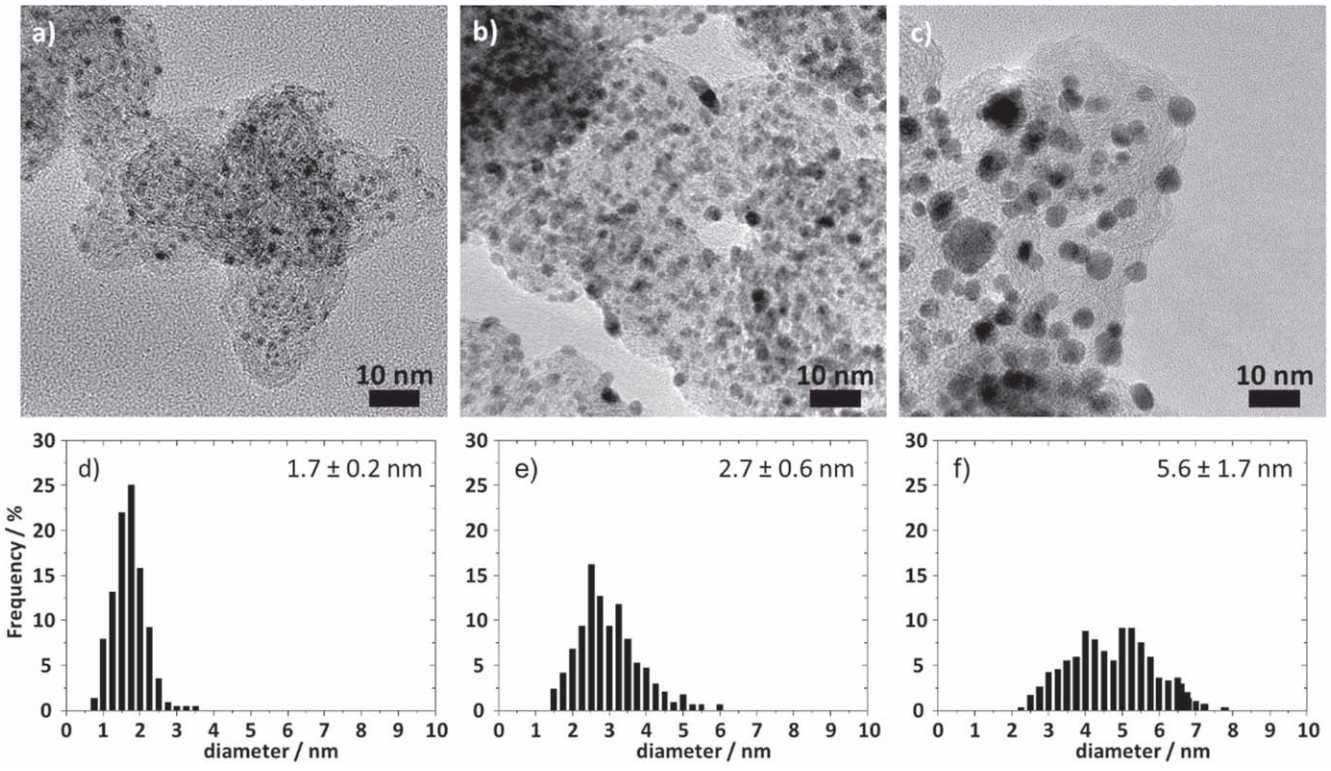

Figure 1. TEM micrographs and size distributions of the commercial 1–2 nm (a), (d), 2–3 nm (b), (e), and 4–5 nm (c), (f) Pt/C catalyst powders.

Table I. Experimental ECSA before and after AST of commercial Pt/C catalysts at T = 25 °C (9000 steps between 0.6 and 1.0 V_{RHE}) and 50 °C (5000 steps between 0.6 and 1.0 V_{RHE}) in oxygen and determined ECSA loss after the AST of three reproducible repeats. The error indicates the standard deviation of the three measurements.

T/°C	Pt/C Catalysts	ECSA/$m^2\ g^{-1}_{Pt}$		surface loss/%
		before AST	after AST	
25	1–2 nm	109 ± 4	62 ± 3	43 ± 1
	2–3 nm	81 ± 1	54 ± 1	34 ± 1
	4–5 nm	57 ± 1	55 ± 1	4 ± 1
50	1–2 nm	90 ± 2	43 ± 2	53 ± 1
	2–3 nm	67 ± 4	35 ± 3	48 ± 2
	4–5 nm	50 ± 2	42 ± 1	16 ± 2

uncompensated resistance leads to larger deviations between "applied and real potential." Nevertheless, the effect should be minor for the upper potential (1.0 V) in the AST as no ORR takes place at this potential. The lower potential (0.6 V), however, should be affected. Consequently, it is difficult to disregard any influence of the uncompensated resistance.

Comparing the GDE studies with different catalyst loading, typically resulting in different film thickness, it can be concluded that although identical trends in stability of the two different catalysts are observed, an extrapolation of the results to fuel cell conditions is more difficult if very thin catalyst films are used since phenomena such as re-deposition of Pt ions do not occur. Therefore, the here presented results highlight the importance of realistic conditions for degradation studies.

Further, crucial mechanistic information concerning the change in the NP size distribution after applying the AST can be extracted from the SAXS data. Representative size distributions are shown in Fig. 3 and repeats in the SI. In the following we refer to the average diameter of the particle and use the standard deviation relative to the evaluation of this average diameter based on three independent measurements as error to compare the catalyst sizes (see Table SI). It should be noticed that in contrast to size histograms plotted in a TEM analysis, minor changes in the fitting parameters lead to deviations in the log-normal plots that might suggest large deviations between the individual measurements. However, we observed that for a given set of conditions, the three individual repeats were consistent: a comparable average diameter and deviation with only small variations between the repeated measurements was observed. For one of the catalyst samples (2–3 nm Pt/C at 50 °C) larger deviations between the individual repeats are observed.

As a result of the AST treatments (at 25 °C or 50 °C) the size distribution (established by SAXS) of all catalysts increases as it is expected from the ECSA loss determined in the CO stripping measurements. For the 1–2 nm Pt/C catalyst the increase in size is most dramatic, an increase from 2.08 ± 0.04 to 4.86 ± 0.43 (AST in O_2 at 25 °C) and 6.06 ± 0.54 nm (AST in O_2 at 50 °C) is determined, while for the 2–3 nm Pt/C catalyst an increase from 2.97 ± 0.09 to 5.24 ± 0.02 (25 °C) and 5.58 ± 1.67 nm (50 °C) is observed. Only the 4–5 nm Pt/C catalyst shows a relative moderate increase in particle size, i.e. from 5.88 ± 0.13 to 6.25 ± 0.47 (25 °C) and 6.63 ± 0.03 nm (50 °C) in line with the very moderate ECSA loss. The size increase of the smaller Pt NPs after the AST is furthermore confirmed by applying PDF analysis (see SI). Interestingly, after applying the AST at 50 °C the "end of treatment" particle sizes of all three Pt/C catalysts are very similar, i.e. they are all in the range of 5.6–6.6 nm. The results demonstrate that, as expected, the degradation and the particle growth are more significant for catalysts with small NPs.[50]

The obtained results are unfortunately difficult to compare to literature as there still no common procedure for AST protocols in RDE measurements, e.g. potential scanning not following the FCCJ protocols was performed on the 2–3 nm Pt /C catalyst on Vulcan C by Kocha et al.[51] (0.025–1.0 V_{RHE}) and on Ketjen black by Mayrhofer et al.[52] (0.4–1.4 V_{RHE}). Speder et al.[19,53] applied load cycles but also on homemade catalysts and Zana et al.[18] performed IL-TEM on homemade catalysts. For MEA measurements the following results are reported: Based on a TEM analysis Yano et al.[54] report that after load cycles in MEA a comparable particle size increase from 2.2 ± 0.5 nm to 6.5 ± 2.3 nm occurs for the 2–3 nm C^{-1} catalyst. Tamaki et al.[55] reported after 10,000 cycles a particle size increase from 3.2 ± 0.8 nm to 7.9 ± 4.6 nm.

In our GDE study, we document for the first time to the best of our knowledge that the "end of treatment" particle size of around 6 nm is rather independent from the "starting size" but depends on the temperature, i.e. after the AST protocol under realistic conditions at 50 °C all three catalysts exhibit more or less the same size distribution. This is an important finding considering that increasing the power density in PEMFCs for mobile applications is of high priority.[8] Currently a large performance loss is observed at high-current density (>1 A cm^{-2}) and it is proposed that a resistive oxygen mass transfer term can be addressed among others through high and stable Pt dispersion (i.e. small NPs).[8] Our results indicate a serious limitation for such efforts to decrease oxygen mass transfer resistances by increasing the catalyst dispersion (i.e. NP size) unless strategies are found and successfully implemented to inhibit the growth in particle size under operation. At the same time the presented GDE methodology provides an easy means to screen test the behavior of different catalysts under realistic conditions.

Focusing on the degradation mechanism, the observed particle size distribution after degradation reported in Fig. 3 is consistent with the established loss in surface area (see Table I). While the surface loss could be in general a consequence of all degradation mechanisms (migration/coalescence, metal dissolution, Ostwald ripening, particle detachment), the observed increase in particle size can occur due to electrochemical Ostwald ripening and particle coalescence. The dependence of the degradation (ECSA loss) on the catalyst layer thickness (catalyst loading on GDL) indicates a significant contribution of electrochemical Ostwald ripening. However, the tail of the size distributions to large sizes (maximum at small size) after the AST at 25 °C could be an indication for coalescence,[56] while tailing to small NP sizes (maximum at large size) after the AST at 50 °C could signify Ostwald ripening.[57,58] The shoulder in the particle size distribution after the AST at 25 °C for 2–3 nm Pt/C, consistent with the "end of treatment size" after the AST at 50 °C, on the other hand might be an indication for coalescence followed by Ostwald ripening into spherical particles under the AST treatment and therefore coalescence might be difficult to detect in the "end of treatment" catalyst. Such a simultaneous occurrence of both growth mechanisms complicates the interpretation of the tailed size distributions[13] and the results do not allow an unambiguous separation of Ostwald ripening and coalescence. To sum up, the strong dependency of the ECSA loss on the catalyst layer thickness makes Ostwald ripening more likely, but coalescence cannot be excluded. Particle detachment, by comparison, leads to a loss in surface area while maintaining the size distribution[52]; a scenario that would best fit to the behavior of the 4–5 nm Pt/C catalyst, but certainly not for the other two catalysts. Mayrhofer et al.[52] showed in IL-TEM that the main degradation mechanism of the 4–5 nm Pt/C catalyst at room temperature and exposure to liquid electrolyte is particle detachment. However, at this point the occurrence of particle detachment in the GDE setup cannot be proven. Metal dissolution (without re-deposition) would lead to a decrease in particle size and is not observed in any of the Pt/C catalysts, i.e. the determined size distributions exhibit very low probability towards small particle sizes. A deposition of the dissolved Pt-ions in the Nafion membrane as observed in MEA measurements seems unlikely, as in the MEA the process is caused by the hydrogen gas crossover.[13] In the GDE measurements, a hydrogen gas crossover through the Nafion membrane is not expected as the measured gas flow at the gas inlet and outlet are

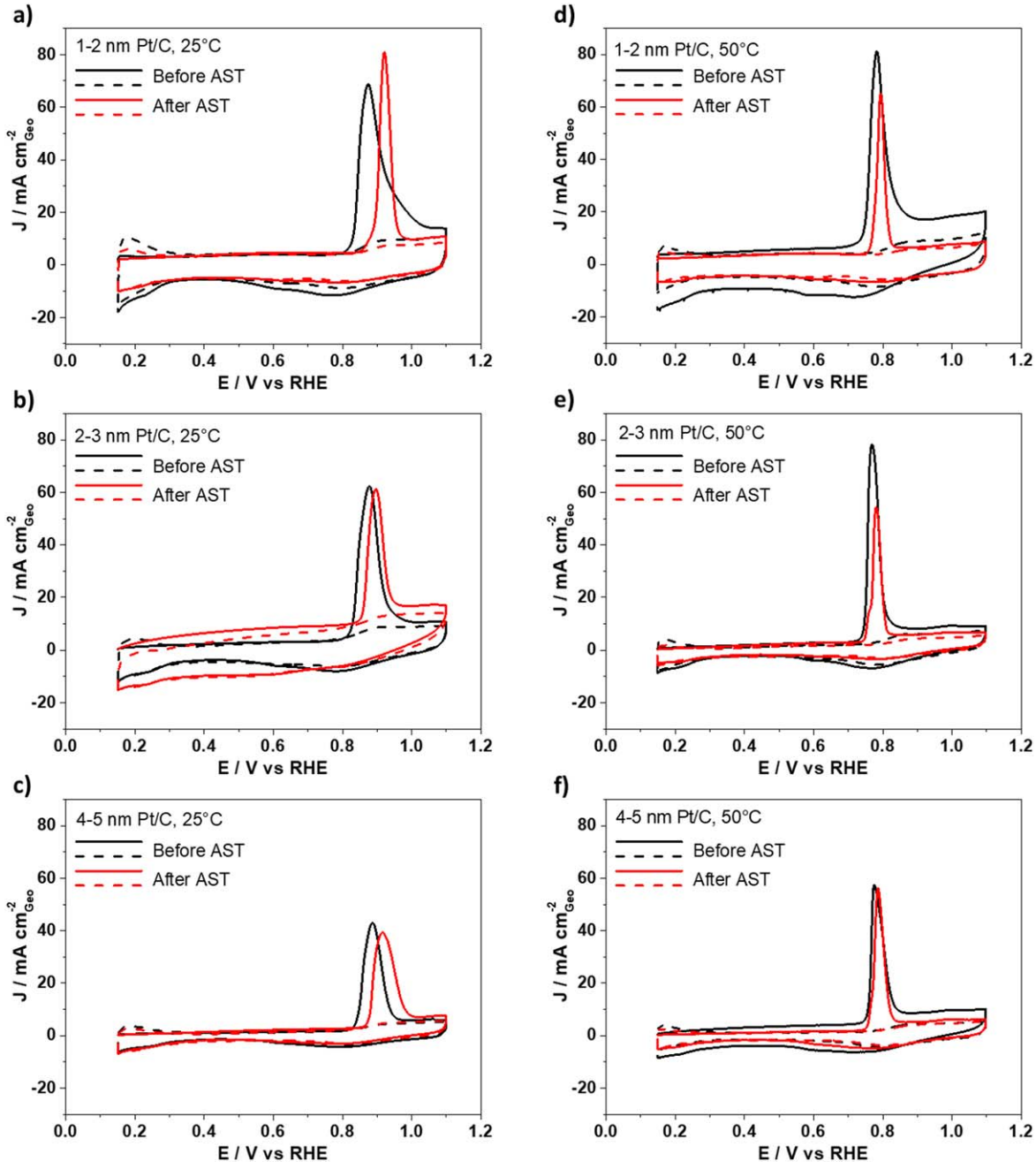

Figure 2. Representative CO stripping curves (solid lines) and subsequent cyclic voltammograms in Ar (dash lines) of commercial 1–2 nm (a), (d), 2–3 nm (b), (e), and 4–5 nm (c), (f) Pt/C catalysts before (black lines) and after (red lines) ASTs in O_2 at 25 °C ((a)–(c) 9000 steps between 0.6 and 1.0 V_{RHE}, 3 s holding) or 50 °C ((d)–(f) 5000 steps between 0.6 and 1.0 V_{RHE}, 3 s holding).

constant and the electrolyte above the membrane is not purged with hydrogen. Therefore, more likely this observation might be related to a (small) component of loss in surface area due to particle detachment.

Conclusions

In summary, in the present work we demonstrate the strength of the application of GDE setups—as compared to classical electrochemical cells or MEAs—for the investigation of catalyst degradation under realistic conditions. In the GDE setup, only one half-cell reaction of a fuel cell, e.g. the oxygen reduction reaction (ORR), is investigated, thus separating anode and cathode degradation. Without further disassembling (as opposed to MEA measurements) or sample collection (in contrast to RDE measurements), the catalyst layer can be investigated by SAXS measurements even without removing the Nafion membrane.

Applying conditions close to MEA testing (regarding the setup,[15] loading,[8] and temperature[4]) the degradation mechanism can be analyzed based on the change in the size distribution and the ECSA obtained by CO stripping. It is found that after applying the ASTs, catalysts with small NPs exhibit significant degradation and particle growth. While this is an expected result, comparing the investigations with previous ones, it is found that the amount of degradation depends on the film thickness; thin films exhibit more degradation than thicker films. The main mechanism seems particle growth based on either coalescence and/or electrochemical Ostwald ripening whereas only for the 4–5 Pt/C catalyst there is a weak indication of particle loss at the applied conditions. The here introduced combination of GDE and SAXS offers a straight-forward

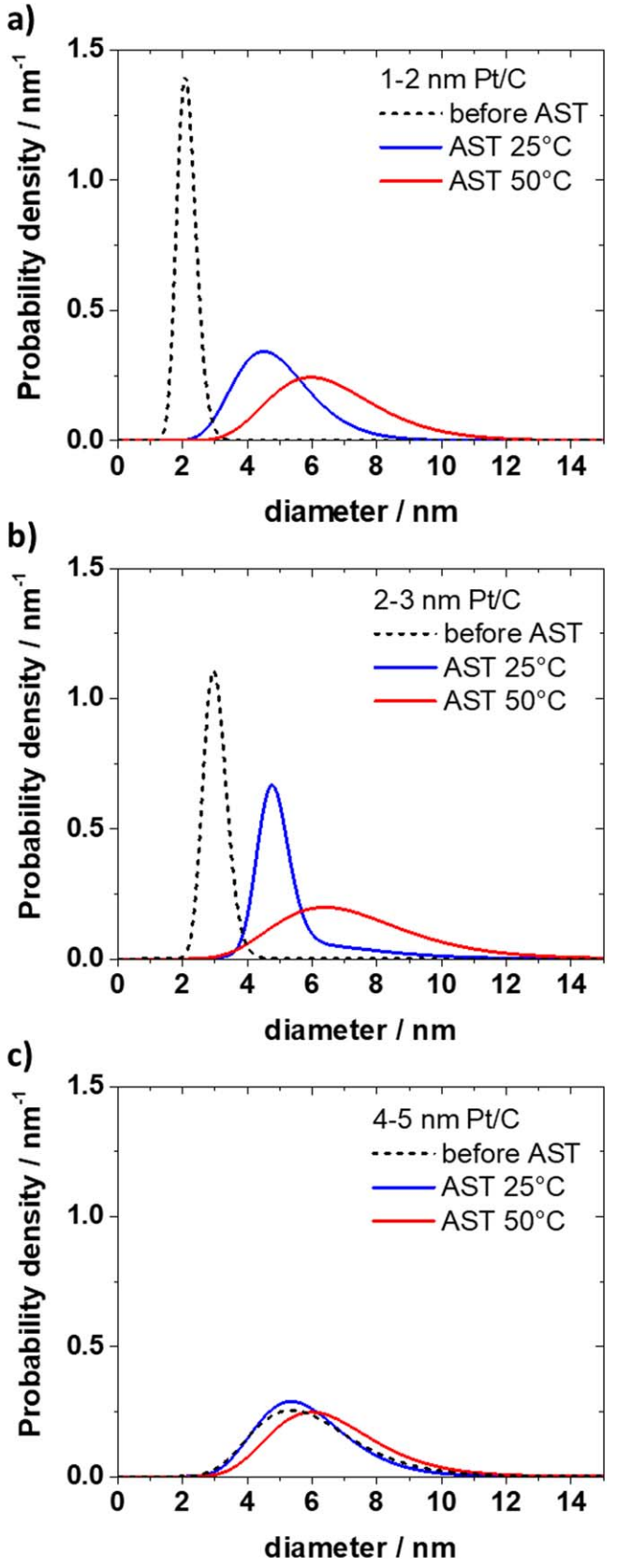

Figure 3. Representative SAXS particle size distributions of commercial 1–2 nm (a), 2–3 nm (b), and 4–5 nm (c) Pt/C catalyst before (dash black lines) and after ASTs in O_2 at 25 °C (blue lines, 9000 steps between 0.6 and 1.0 V_{RHE}, 3 s holding) or 50 °C (red lines, 5000 steps between 0.6 and 1.0 V_{RHE}, 3 s holding).

way for comparative studies of the degradation of several different fuel cell catalysts allowing several repeats. The approach therefore offers significant advantages over RDE and MEA measurements and thus will aid the quest for developing improved PEMFC catalysts.

Acknowledgments

This work was supported by the Swiss National Science Foundation (SNSF) via the project No. 200021_184742. J.S. acknowledges the German Research Foundation (DFG) for financial support (KU 3152/6–1) and the German Academic Exchange Service (DAAD) for financial support through a scholarship for an academic exchange to the University of Bern. J.Q and K.M.Ø.J thank the Villum foundation for financial support through a Villum Young Investigator grant. J.Q. and M.A. thank Dr Luise Theil Kuhn and Dr Søren B. Simonsen, technical University of Denmark (DTU) for access to TEM facilities. J.Q., K.M.Ø.J. and J.J.K.K. acknowledge local support and continued access to the University of Copenhagen SAXSLab facility. Use of the Advanced Photon Source was supported by the U. S. Department of Energy, Office of Science, Office of Basic Energy Sciences, under Contract No. DE-AC02–06CH11357 (proposal GUP-65450).

ORCID

Johanna Schröder https://orcid.org/0000-0001-5461-4751

References

1. I. Katsounaros, S. Cherevko, A. R. Zeradjanin, and K. J. J. J. Mayrhofer, *Angew. Chemie - Int. Ed.*, **53**, 102 (2014).
2. T. Reier et al., *J. Am. Chem. Soc.*, **137**, 13031 (2015).
3. M. K. Debe, *Nature*, **486**, 43 (2012).
4. T. Yoshida and K. Kojima, *Electrochem. Soc. Interface*, **24**, 45 (2015).
5. V. R. Stamenkovic, B. S. Mun, M. Arenz, K. J. J. Mayrhofer, C. A. Lucas, G. Wang, P. N. Ross, and N. M. Markovic, *Nat. Mater.*, **6**, 241 (2007).
6. D. Wang, H. L. Xin, R. Hovden, H. Wang, Y. Yu, D. A. Muller, F. J. DiSalvo, and H. D. Abruña, *Nat. Mater.*, **12**, 81 (2013).
7. B. Han, C. E. Carlton, A. Kongkanand, R. S. Kukreja, B. R. Theobald, L. Gan, R. O'Malley, P. Strasser, F. T. Wagner, and Y. Shao-Horn, *Energy Environ. Sci.*, **8**, 258 (2015).
8. A. Kongkanand and M. F. Mathias, *J. Phys. Chem. Lett.*, **7**, 1127 (2016).
9. A. Marcu, G. Toth, S. Kundu, L. C. Colmenares, and R. J. Behm, *J. Power Sources*, **215**, 266 (2012).
10. A. Ohma, K. Shinohara, A. Iiyama, T. Yoshida, and A. Daimaru, *ECS Trans.*, **41**, 775 (2019).
11. Y.-C. Park, K. Kakinuma, M. Uchida, D. A. Tryk, T. Kamino, H. Uchida, and M. Watanabe, *Electrochim. Acta*, **91**, 195 (2013).
12. T. Nagai, H. Murata, and Y. Morimoto, *J. Electrochem. Soc.*, **161**, F789 (2014).
13. P. J. Ferreira et al., *J. Electrochem. Soc.*, **152**, A2256 (2005).
14. M. Inaba, A. W. Jensen, G. W. Sievers, M. Escudero-Escribano, A. Zana, and M. Arenz, *Energy Environ. Sci.*, **11**, 988 (2018).
15. S. Alinejad, M. Inaba, J. Schröder, J. Du, J. Quinson, A. Zana, and M. Arenz, *J. Phys.: Energy*, **2**, 024003 (2020).
16. J. C. Meier, C. Galeano, I. Katsounaros, A. A. Topalov, A. Kostka, F. Schüth, and K. J. J. Mayrhofer, *ACS Catal.*, **2**, 832 (2012).
17. K. Hartl, M. Hanzlik, and M. Arenz, *Energy Environ. Sci.*, **4**, 234 (2011).
18. A. Zana, J. Speder, M. Roefzaad, L. Altmann, M. Bäumer, and M. Arenz, *J. Electrochem. Soc.*, **160**, F608 (2013).
19. J. Speder, A. Zana, I. Spanos, J. J. K. K. Kirkensgaard, K. Mortensen, M. Hanzlik, and M. Arenz, *J. Power Sources*, **261**, 14 (2014).
20. J. Speder, L. Altmann, M. Roefzaad, M. Bäumer, J. J. K. K. Kirkensgaard, K. Mortensen, and M. Arenz, *Phys. Chem. Chem. Phys.*, **15**, 3602 (2013).
21. V. Yarlagadda, S. E. McKinney, C. L. Keary, L. Thompson, B. Zulevi, and A. Kongkanand, *J. Electrochem. Soc.*, **164**, F845 (2017).
22. G. K. H. Wiberg, K. J. J. Mayrhofer, and M. Arenz, *Fuel Cells*, **10**, 575 (2010).
23. M. Inaba, J. Quinson, J. R. Bucher, and M. Arenz, *J. Vis. Exp.*, **133**, e57105 (2018).
24. J. Quinson et al., *ACS Catal.*, **8**, 6627 (2018).
25. T. Zemb and P. Lindner, *Neutron, X-rays and Light. Scattering Methods Applied to Soft Condensed Matter*, ed. T. Zemb and P. Lindner (Elsevier, Amsterdam) p. 552 (2002).
26. K. Kajiwara and Y. Hiragi, *Analytical Spectroscopy Library*, **7**, 353 (1996).
27. P. R. A. F. Garcia, O. Prymak, V. Grasmik, K. Pappert, W. Wlysses, L. Otubo, M. Epple, and C. L. P. Oliveira, *Nanoscale Adv.*, **2**, 225 (2020).
28. P. J. Chupas, X. Qiu, J. C. Hanson, P. L. Lee, C. P. Grey, and S. J. L. Billinge, *J. Appl. Crystallogr.*, **36**, 1342 (2003).
29. A. P. Hammersley, S. O. Svensson, M. Hanfland, A. N. Fitch, and D. Häusermann, *High Press. Res.*, **14**, 235 (1996).
30. A. P. Hammersley, *J. Appl. Crystallogr.*, **49**, 646 (2016).
31. X. Yang, P. Juhas, C. L. Farrow, and S. J. L. Billinge, (2014), arXiv:http://arxiv.org/abs/1402.3163.

32. C. L. Farrow, P. Juhas, J. W. Liu, D. Bryndin, E. S. Boin, J. Bloch, T. Proffen, and S. J. L. Billinge, *J. Phys. Condens. Matter*, **19**, 335219 (2007).
33. S. Mitsushima, Y. Koizumi, S. Uzuka, and K.-I. Ota, *Electrochim. Acta*, **54**, 455 (2008).
34. J. Omura, H. Yano, M. Watanabe, and H. Uchida, *Langmuir*, **27**, 6464 (2011).
35. T. Lopes, J. Chlistunoff, J.-M. Sansiñena, and F. H. Garzon, *Int. J. Hydrogen Energy*, **37**, 5202 (2012).
36. Y. Furuya, T. Mashio, A. Ohma, M. Tian, F. Kaveh, D. Beauchemin, and G. Jerkiewicz, *ACS Catal.*, **5**, 2605 (2015).
37. A. A. Topalov, S. Cherevko, A. R. Zeradjanin, J. C. Meier, I. Katsounaros, and K. J. J. Mayrhofer, *Chem. Sci.*, **5**, 631 (2014).
38. K. N. Wood, S. T. Christensen, S. Pylypenko, T. S. Olson, A. A. Dameron, K. E. Hurst, H. N. Dinh, T. Gennett, and R. O'hayre, *MRS Commun.*, **2**, 85 (2012).
39. T. Binninger et al., *J. Electrochem. Soc.*, **163**, H906 (2016).
40. M. Povia, J. Herranz, T. Binninger, M. Nachtegaal, A. Diaz, J. Kohlbrecher, D. F. Abbott, B.-J. Kim, and T. J. Schmidt, *ACS Catal.*, **8**, 7000 (2018).
41. J. A. Gilbert, N. N. Kariuki, R. Subbaraman, A. J. Kropf, M. C. Smith, E. F. Holby, D. Morgan, and D. J. Myers, *J. Am. Chem. Soc.*, **134**, 14823 (2012).
42. H.-G. G. Haubold, X. H. Wang, G. Goerigk, and W. Schilling, *J. Appl. Crystallogr.*, **30**, 653 (1997).
43. J. Tillier, T. Binninger, M. Garganourakis, A. Patru, E. Fabbri, T. J. Schmidt, and O. Sereda, *J. Electrochem. Soc.*, **163**, H913 (2016).
44. X. Tuaev, S. Rudi, V. Petkov, A. Hoell, and P. Strasser, *ACS Nano*, **7**, 5666 (2013).
45. M. Nesselberger, S. Ashton, J. C. Meier, I. Katsounaros, K. J. J. Mayrhofer, and M. Arenz, *J. Am. Chem. Soc.*, **133**, 17428 (2011).
46. E. Herrero, J. M. Feliu, S. Blais, Z. Radovic-Hrapovic, and G. Jerkiewicz, *Langmuir*, **16**, 4779 (2000).
47. M. Inaba, J. Quinson, and M. Arenz, *J. Power Sources*, **353**, 19 (2017).
48. G. P. Keeley, S. Cherevko, and K. J. J. Mayrhofer, *ChemElectroChem*, **3**, 51 (2016).
49. O. Kasian, S. Geiger, K. J. J. Mayrhofer, and S. Cherevko, *Chem. Rec.*, **19**, 2130 (2019).
50. E. F. Holby, W. Sheng, Y. Shao-Horn, and D. Morgan, *Energy Environ. Sci.*, **2**, 865 (2009).
51. S. S. Kocha, K. Shinozaki, J. W. Zack, D. J. Myers, N. N. Kariuki, T. Nowicki, V. Stamenkovic, Y. Kang, D. Li, and D. Papageorgopoulos, *Electrocatalysis*, **8**, 366 (2017).
52. K. J. J. Mayrhofer, J. C. Meier, S. J. Ashton, G. K. H. Wiberg, F. Kraus, M. Hanzlik, and M. Arenz, *Electrochem. Commun.*, **10**, 1144 (2008).
53. J. Speder, A. Zana, I. Spanos, J. J. K. K. Kirkensgaard, K. Mortensen, and M. Arenz, *Electrochem. Commun.*, **34**, 153 (2013).
54. H. Yano, M. Watanabe, A. Iiyama, and H. Uchida, *Nano Energy*, **29**, 323 (2016).
55. T. Tamaki, A. Minagawa, B. Arumugam, B. A. Kakade, and T. Yamaguchi, *J. Power Sources*, **271**, 346 (2014).
56. C. G. Granqvist and R. A. Buhrman, *J. Appl. Phys.*, **47**, 2200 (1976).
57. A. Baldan, *J. Mater. Sci.*, **37**, 2379 (2002).
58. Y. Zhai, H. Zhang, D. Xing, and Z.-G. Shao, *J. Power Sources*, **164**, 126 (2007).